PAPER

A feasibility study of high-strength Bi-2223 conductor for high-field solenoids

IOP Publishing Superconductor Science and Technology
Supercond. Sci. Technol. 30 (2017) 035011 (15pp) https://doi.org/10.1088/1361-6668/aa5582

A feasibility study of high-strength Bi-2223 conductor for high-field solenoids

A Godeke[1], D V Abraimov, E Arroyo, N Barret, M D Bird, A Francis, J Jaroszynski, D V Kurteva, W D Markiewicz, E L Marks, W S Marshall, D M McRae, P D Noyes, R C P Pereira, Y L Viouchkov, R P Walsh and J M White

National High Magnetic Field Laboratory, 1800 East Paul Dirac Drive, Tallahassee, FL 31310, USA

E-mail: arno.godeke@varian.com

Received 11 October 2016, revised 20 December 2016
Accepted for publication 22 December 2016
Published 30 January 2017

Abstract

We performed a feasibility study on a high-strength $Bi_{2-x}Pb_xSr_2Ca_2Cu_3O_{10-x}$(Bi-2223) tape conductor for high-field solenoid applications. The investigated conductor, DI-BSCCO Type HT-XX, is a pre-production version of Type HT-NX, which has recently become available from Sumitomo Electric Industries. It is based on their DI-BSCCO Type H tape, but laminated with a high-strength Ni-alloy. We used stress–strain characterizations, single- and double-bend tests, easy- and hard-way bent coil-turns at various radii, straight and helical samples in up to 31.2 T background field, and small 20-turn coils in up to 17 T background field to systematically determine the electro-mechanical limits in magnet-relevant conditions. In longitudinal tensile tests at 77 K, we found critical stress- and strain-levels of 516 MPa and 0.57%, respectively. In three decidedly different experiments we detected an amplification of the allowable strain with a combination of pure bending and Lorentz loading to $\geqslant$0.92% (calculated elastically at the outer tape edge). This significant strain level, and the fact that it is multi-filamentary conductor and available in the reacted and insulated state, makes DI-BSCCO HT-NX highly suitable for very high-field solenoids, for which high current densities and therefore high loads are required to retain manageable magnet dimensions.

Keywords: high temperature superconductor, $Bi_2Sr_2Ca_2Cu_3O_{10x}$ (Bi-2223), high field solenoid, NMR, magnet

(Some figures may appear in colour only in the online journal)

1. Introduction

The National Research Council's (NRC) Committee on Opportunities in High Magnetic Field Science's 2005 'COHMAG' report [1], as well as the NRC's Committee to Assess the Current Status and Future Direction of High Magnetic Field Science in the United States' 'MagSci' report [2] describe a number of science drivers for the development of very high-field solenoids. Amongst these are:

- Create regional 32 T superconducting magnets at three to four locations.
- Establish at least three US 1.2 GHz NMR instruments.
- Plan for 1.5 GHz NMR system development.
- Establish high-field (≈30 T) facilities for neutron and photon scattering.
- Construct a 20 T MRI instrument.
- Construct a 40 T all-superconducting magnet.
- Construct a 60 T DC hybrid magnet.

It is evident from this list that there is a large demand for solenoids in the magnetic field range of 30 T and higher. The industry workhorse materials for very high-field solenoids are the low temperature superconductors (LTS) Nb–Ti and

[1] Present address: Varian Medical Systems Particle Therapy GmbH, Mottmannstr. 2, D-53842 Troisdorf, Germany.

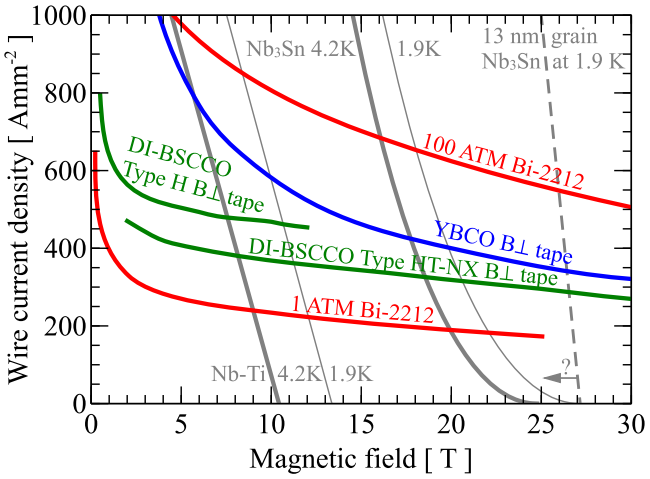

Figure 1. Comparison of critical currents as a function of magnetic field at 4.2 K (unless otherwise depicted) of commercially available superconductors for high-field solenoids: Nb–Ti and Nb_3Sn wires [4] (data reproduced with permission from IEEE, © source article 2007), DI-BSCCO Type H tape [11] (data reproduced with permission from H. Kitaguchi and Elsevier, © source article 2008), 1 atmosphere reacted Bi-2212 wire [12] (data reproduced with permission from IOP Publishing, © source article 2010), 100 atmosphere reacted Bi-2212 wire [13], YBCO tape [13] (data from [13] are reproduced with permission from Macmillan Publishers Ltd: Nature Materials, © source article 2014), and DI-BSCCO Type HT-NX (this work). Continuous lines are parameterizations of measured data and the dashed line is a calculated estimate as described in the main text.

Nb_3Sn . However, the highest magnetic field that is available with LTS materials is 23.5 T [3]. One can estimate the current-density that is required in the windings of such a magnet from $J_w \approx B(0.85\mu_0(r_{out} - r_{in}))^{-1}$, in which B is the axial magnetic field, $\mu_0 = 4\pi \times 10^{-7}$ Hm^{-1}, and r_{out} and r_{in} are the outer and inner radii of the windings, respectively. This leads, for a generic $r_{out} = 300$ mm and $r_{in} = 30$ mm, to $J_w \approx 81$ A mm^{-2}, or, if conductor insulation and packing efficiency are accounted for, to a conductor (engineering) current-density on the order of $J_E \approx 100 - 150$ A mm^{-2}.

When comparing this current-density with the performance of modern high-current LTS conductors [4–6] (figure 1), it is clear that 23.5 T is at the limit of what is presently achievable with LTS. The key origin of this performance limitation is intrinsic and determined by the upper critical field (B_{c2}) of Nb_3Sn of 30 T [7]. The high-field critical current-density of Nb_3Sn wires can in principle be improved significantly by reducing the grain-size to around 10–20 nm and thereby improving the high-field pinning efficiency [8, 9], and this potential can be estimated (figure 1). Such fine-grain wires are presently not commercially available, although promising results have been demonstrated [10].

To generate magnetic fields above 23.5 T, one has therefore to use inserts that are constructed either from resistive materials, or from one of the commercially available 'high temperature' superconductors (HTS): $Bi_2Sr_2CaCu_2O_{8+x}$ (Bi-2212), $Bi_{2-x}Pb_xSr_2Ca_2Cu_3O_{10-x}$ (Bi-2223), or (RE)$Ba_2Cu_3O_{7-\delta}$ (REBCO, where RE is a Rare Earth element) that have magnetic field limits at 4.2 K that are substantially above 100 T [13].

REBCO has been a main candidate conductor for many laboratories due to its high current-density [13] and intrinsic strength [14, 15] (which is required for compact magnets [16]), the fact it does not require a reaction, and its availability from more than six manufacturers. The maximum allowable longitudinal strain before I_c degradation occurs is around 0.65%, at stress levels of 600–800 MPa depending on the Cu-thickness [14, 17, 18]. There are currently a number of magnets that have reached fields beyond 23.5 T [14, 19–21], a special cryogen-free magnet [22], and a 32 T user magnet that is planned for early 2017 [14, 19]. Though REBCO exhibits electronic anisotropy [6, 13] that somewhat complicates its application, the current-density in the 'bad' direction ($B \perp ab$) is sufficiently high for 30 T and higher-field solenoid applications (figure 1). A major concern for NMR applications are 'screening currents' that result from the conductor not being multi-filamentary, but substantial efforts are made to mitigate the resulting field-inhomogeneities [16, 23, 24].

Bi-2212 is an interesting candidate material due to the fact that it is the only commercial HTS conductor that is available as a round wire with twisted filaments and a bi-axial melt-growth texture [25]. A disadvantage of Bi-2212 is that it has to be reacted after coil winding at around 888 °C within only a few degrees Celsius in an oxygen-rich environment, which places strict demands on the insulation and coil-former materials. Moreover, to achieve the high current densities that are required to allow for sufficient margin for adding reinforcement to the mechanically relatively weak conductor, the reaction needs to take place at 25–100 bar in an oxygen-inert gas mixture [13, 26] (figure 1). There is presently discrepancy in the literature on whether densification of the Bi-2212 by overpressure reaction improves the allowable longitudinal strain limit beyond the 0.3%–0.4% that is commonly observed in Ag/Ag-alloy matrix Bi-2212 and Bi-2223 wires and tapes [27–35]: Substrate-based experiments suggest no improvement and a 0.3%–0.4% strain limit, whereas tensile tests suggest a 0.6% strain limit [36–39]. That Bi-2212 is mechanically-weaker than both REBCO and high-strength Bi-2223 (below) is clear and there are recent attempts to diffusion-bond high-strength materials to aspected Bi-2212 wires to improve the allowable tensile stress from 120 to 150 MPa [39, 40] to more than 400 MPa [40]. Despite the strength- and reaction-difficulties, Bi-2212 has major advantages for high-resolution NMR magnets, and significant progress has been made to address the technological issues [13, 41–44].

The focus of this paper is on Bi-2223, which was the first commercially available HTS conductor in the mid 1990s. It is a tape conductor with anisotropic properties but has, similar to REBCO, sufficient current-density in the 'bad' field direction ($B \perp ab$, figure 1). Grain texture and high density are achieved by rolling and reaction under pressure but, in contrast to Bi-2212, the conductor is available in reacted form. Similar to Bi-2212, the brittle superconducting grains are embedded in a mechanically-weak Ag/Ag-alloy matrix. In

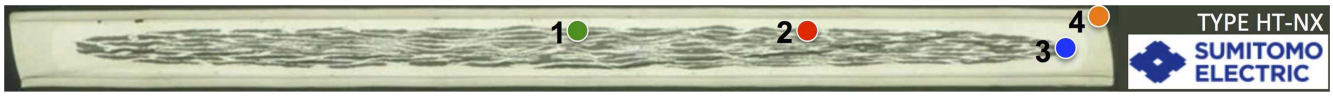

Figure 2. Cross-section of a 4.5 × 0.26 mm^2 high-strength Ni-alloy laminated DI-BSCCO Type HT-NX conductor, courtesy of Sumitomo Electric Industries. Indicated are the locations of maximum longitudinal strain on the filaments resulting from hard-way bending (3, blue), easy-way bending (1, green) and the maximum longitudinal strain (2, red). The location of the maximum strain in the lamination as a result of combined hard- and easy-way bending is also indicated (4, orange).

Bi-2223, however, the mechanical properties are substantially improved [34, 35] (while retaining performance [45]) by soldering pre-tensioned stainless-steel (SS) or copper alloys (CA) onto the reacted tape. This lamination process was pioneered at American Superconductor Corporation [46, 47] and further optimized and commercialized by Sumitomo Electric Industries (SEI). Sumitomo uses the product names DI-BSCCO HT-SS and DI-BSCCO HT-CA for laminated versions of their bare DI-BSCCO Type H tape. The allowable stresses in type HT-SS and HT-CA (270 MPa and 250 MPa respectively [48]) are drastically improved compared to the bare conductor. The allowable strain, however, is still limited by the yield strain of the lamination, i.e. on the order of 0.35% and therefore comparable to the strain limit of the bare conductor. This may be undesired in a reacted conductor, for which much of the tensile strain-margin can be consumed by bending strain. It is therefore better to laminate with a material that has a high Young's modules in combination with a high elastic strain limit. Despite this limited strain-margin, there have been a number of successful attempts to construct magnets from the SS- and CA-laminated conductors. Examples are a 20 T cryogen-free magnet [49] and three LTS/Bi-2223 magnets that have successfully generated an NMR signal [50–53]. Amongst these is a 1020 MHz (24 T) system [53], which is the present record for very high-field NMR.

In 2014 SEI announced the availability of DI-BSCCO Type HT-NX (figure 2; pre-production versions were named HT-XX), which is laminated with a high-strength Ni-alloy and has a reported strain- and stress-limit of 0.57% and 443 MPa, respectively [54]. Attractive properties [54, 55], promising findings from other evaluations [48, 56, 57], and early suggestions of even higher strain limits in bending (allowable bending diameters between 20 and 30 mm [55] and unexpected-high load-performance under hoop stress [57]) triggered us to perform a systematic feasibility study on the suitability of DI-BSCCO HT-NX material for very high-field solenoids.

2. Experiments

A summary of the strain patterns that occur in high-field solenoids wound from Bi-2223 tape is sketched in figure 3. Experiments were designed to systematically investigate the effect and limits of the individual strain components in order to determine design limits for future magnets, and to enable comparisons with the alternative HTS conductors. All tests were performed on a 100 m pre-production batch with SEI identification DI-BSCCO HT-XX.

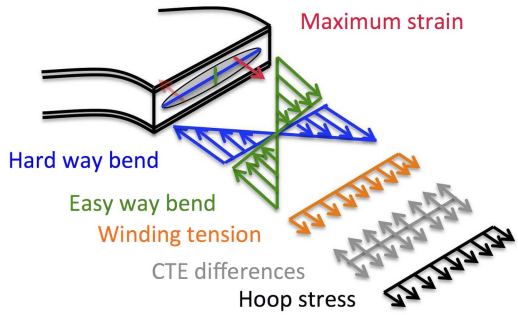

Figure 3. Various longitudinal strain components that occur as a result of hard- and easy-way bending, tension on the conductor during winding, differences in the coefficient of thermal expansion (CTE) and Lorentz load during magnet excitation. Also indicated is the location of the maximum longitudinal strain on the filaments.

2.1. Longitudinal tensile tests at 77 K

Tensile tests at 77 K were performed to determine the basic mechanical properties of the conductor. For this experiment the tapes were clamped between Al-alloy bolt-together grips without making the cross-section of the central region smaller, i.e. dog-boning. The load was measured with a load-cell and displacement with a 50 mm gauge-length cryogenic clip-on extensometer. Two tapes were tested and very high reproducibility was observed. For a third sample the I_c as a function of stress (σ) was measured using copper tensile grips. Tape samples were delaminated using a hot plate and tensile tests were performed at 77 K on the lamination and on the bare tape, again without dog-boning the samples.

2.2. Thermal contraction from 295 to 4.2 K

The thermal contraction from 295 to 4.2 K was measured using a cryogenic tube-type, 2 specimen stage dilatometer in which the thermal contraction of the test sample is compared to a known reference sample. A suitable sample geometry was created by stacking 10 tape-sections of about 50 mm length together and milling the ends. The repeatability was investigated by testing the sample multiple times. Equipment issues unfortunately led to a relatively large uncertainty of ±0.03% in the resulting thermal contraction data.

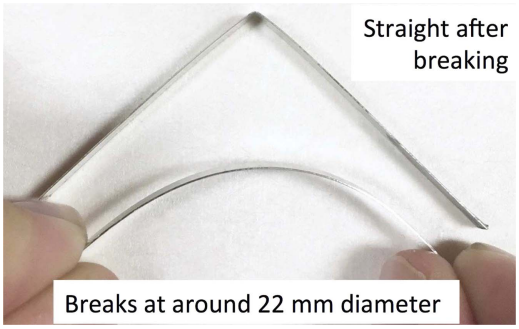

Figure 4. A conductor that is bend at room-temperature, and a conductor after failure due to room-temperature bending.

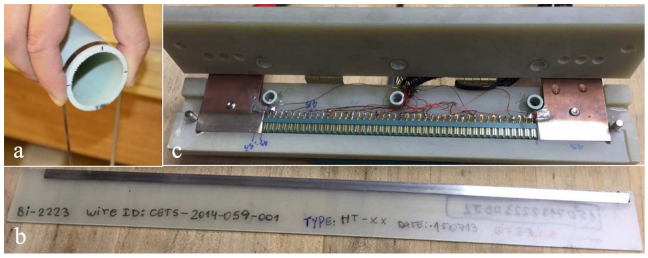

Figure 5. Single- and double-bend test procedure (a), straightened tape-sample after a single- or double-bend (b), and a clamp with a voltage-tap array to measure the I_c as a function of position at 77 K (c).

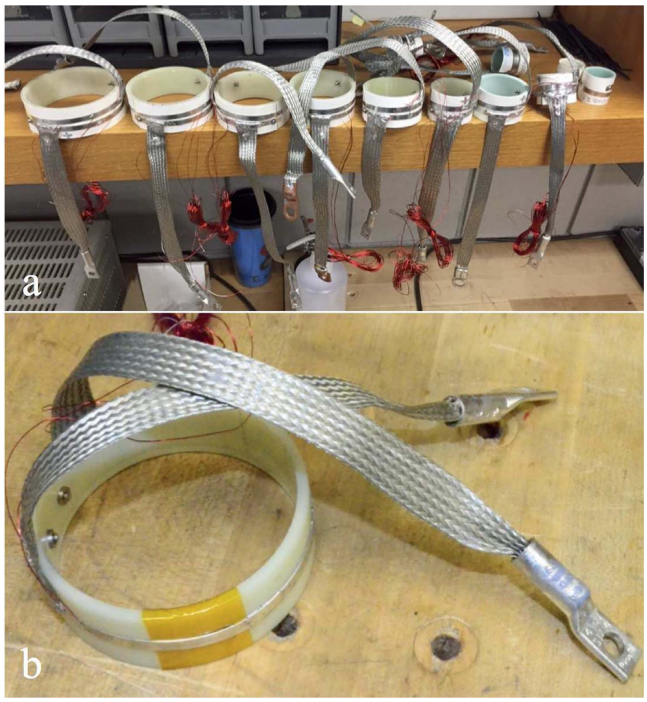

Figure 6. Single- and hard-way bent test-coil sections (a) and a curved splice sample (b).

2.3. Room-temperature bend-tests

Although standards for the effect of bending on the critical-current of Bi-2223 tapes have been established in the literature [58, 59], we decided to develop our own procedures for such tests. A large number of room-temperature bend-tests were performed, ranging from a simple tape bend-test (figure 4), single- and double bend-tests around a former (figure 5), to coil-sections that contain either an easy-way bend or an easy-way bend plus a hard-way s-bend (figure 6(a)).

2.3.1. Single- and double-bend tests. We performed double-bend tests at 76.3, 70.1, 63.6, 57.2, 50.7, 44.5, 38.1, 31.6, 25.4, and 22.1 mm diameter to determine the minimum diameter at which the I_c starts to degrade. In the double-bend tests, an approximately 15 cm long tape-section was bent in the middle, first in one direction around a mandrel (figure 5(a)), straightened, then bent in the opposite direction, straightened, and mounted on a G10 strip (figure 5(b)) using 3M^{TM} high-temperature silicone-adhesive transfer-tape which provides consistent glue thickness and is, from experience, cryogenically compatible. G10 is selected as a sample carrier since it closely matches the thermal contraction of the HT-XX tape (see section 3.1) and therefore does not strain the sample during cooldown. A clamp was developed with a voltage-tap array with a spacing of 4 mm and two current terminals. The clamp enables high-throughput I_c measurements as a function of position along the tape at 77 K (figure 5(c)).

After double-bending and G10-strip mounting, a sample is clamped and the I_c is measured across sequential 16 mm sections. The results give both an impression of the variation of I_c along the length of the tape-section, as well as a potentially reduced I_c for the central tape-section that has been bent. The single-bend experiment, performed for 50.7, 44.5, 38.1, 31.6, 25.4, and 22.1 mm diameters is identical apart from not bending the tape-sample in the opposite direction and measuring the I_c before bending as well. It is important to note that one sample is used for each diameter, both in the single-bend and well as in the double-bend experiments.

2.3.2. Easy- and easy-plus hard-way bent coil-sections. To investigate the onset of I_c reduction as a result of bending-strain during coil-winding, we created two sets of coil-sections at 76.3, 70.1, 63.6, 57.2, 50.7, 44.5, 38.1, 31.6, 25.4, and 22.1 mm diameter (figure 6(a)). In one coil set, the conductor is wound helically with a single pitch, thereby imposing an easy-way bend that is representative for the central section of a coil. In a second coil set, the conductor is wound helically with a single pitch plus an s-bend, which is representative for the end of a layer-wound coil where the conductor has to reverse direction. Again, G10 coil-formers are used that closely match the thermal contraction of the tape. The tape path is enforced using Nomex® paper that is cut to shape using a Silhouette Cameo® crafts paper-cutter driven by 3D-CAD software. The ends of the tape-sections are fixed with a small bolt, and voltage and current contacts are soldered with a temperature-controlled soldering iron which is followed by an I_c measurement at 77 K. Mounting current- and voltage-contacts for diameters below 30 mm was

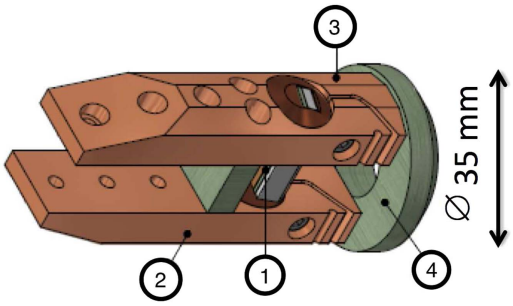

Figure 7. Variable field-angle sample holder to measure $I_c(B, \phi)$ on 35 mm tape-samples. 1: sample; 2: current connection; 3: clamp system enabling room temperature angle adjustment; 4: guide cone and support.

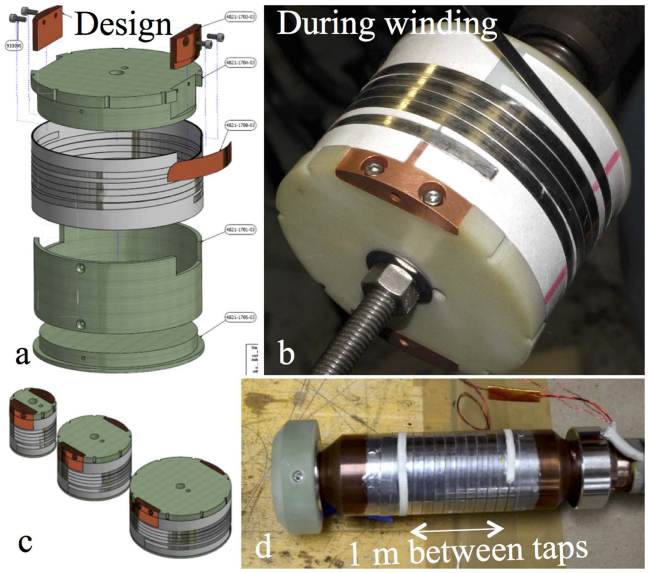

Figure 8. Coil and helical sample holder. (a) Coil design; (b) coil fabrication; (c) 51, 83, and 114 mm diameter coils; (d) helical sample holder.

not possible since the local thermal-strain that is introduced by the soldering iron, which is additive to the bending-strain, caused the tape to break.

2.4. Splice resistances

The unit-length of DI-BSCCO is quickly increasing with a present availability of 300 m length and an expected unit-length of 500 m in the near future [60]. Despite this rapid progress, it is expected that a number of splices will have to be made in future applications. The Ni-alloy lamination increases the contact-resistance when left in place, and removal of the lamination before splicing is non-trivial due to the pre-tension that causes mechanical discontinuities if the lamination is removed. Although low-resistance splice methods are under development [60], it is not trivial to implement such methods in solenoids with a small inner winding-diameter where bending a spliced conductor would increase the bending-strain to unacceptable levels. We have therefore developed a method to solder the tapes together after bending, and make curved splices without removal of the Ni-alloy lamination. We used curved splice-sections as shown in figure 6(b) to determine the splice-resistance as a function of splice-length.

2.5. Critical-current measurements up to 31.2 T

The critical-current as a function of field and field-angle ($I_c(B, \phi)$) at 4.2 K over the relevant magnetic field range is required for coil design and optimization. New sample holders were developed to measure $I_c(B, \phi)$ on short straight samples (figure 7) as well as on 1.2 m long helical samples (figure 8(d)). The critical currents were determined at an electric-field criterion of $E_c = 100\ \mu\mathrm{Vm}^{-1}$ and the n-value was obtained from a fit of the transition to $E = E_0 + RI/l + E_c(I/I_c)^n$, in which E_0 is an offset, R is a possible resistive component, and l is the distance between the voltage taps.

2.5.1. Short straight samples. Sample holders were fabricated for the 52 mm bore of a 15 T superconducting solenoid as well as for a 50 mm warm bore 31.2 T resistive magnet with a 38 mm bore cryostat. The sample length for the 15 T system is 45 mm with a 10 mm voltage-tap separation, whereas the sample length for the 31.2 T system is 35 mm with a 7 mm voltage-tap separation. In two sample holders the sample is fixed with the magnetic field either perpendicular to the broad side of the tape ($B \perp ab$) or parallel ($B \parallel ab$). In a third sample holder, the sample angle is adjustable with respect to the background magnetic field (figure 7). The angle adjustment in the holder used for the present analysis is made at room-temperature, but a new holder that can be adjusted while the sample remains cold is currently under development. The availability of three independent holders enables a faster sample exchange in the limited high-field resistive magnet time. $I_c(B, \phi)$ was measured up to 15 T for angles between the magnetic field and the ab-plane $\phi = 0°$, 7°, 17°, 27°, 34°, 46°, 68°, and 91°. Due to time constraints only a select set of angles close to $B \parallel ab$ and including $B \perp ab$ ($\phi = 0°$, 4°, 10°, 15°, 21°, and 90°) were measured up to 31.2 T since these are the most critical for magnet design.

2.5.2. Long helical samples. The short samples in section 2.5.1 are effective for material development and rapid characterization, but longer samples are generally more suitable for coil performance analyses. It is common practice in LTS to judge magnet-relevant conductor performance using about 1.2 m long helical samples that are mounted on Ti–6Al–4V so-called ITER barrels [61, 62]. We have created similar helical sample holders that are based on a method that was developed at Lawrence Berkeley National Laboratory [63], but now using a 37 mm G10-tube holder equipped with press-fitted copper current connections as shown in figure 8(d). The tape geometry only allows for a measurement in which the field is parallel to the ab plane. The fact that the current is not perfectly perpendicular to the field as a result of the pitch is ignored here. The tape sample is helically-wound onto the G10-tube holder using Nylon wire

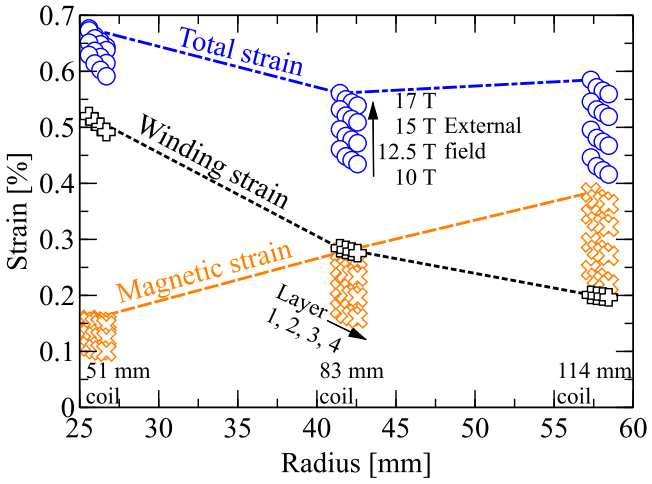

Figure 9. Designed winding, magnetic, and total strain-levels at the estimated critical-current on the outside of the conductor across the layers at various background magnetic field levels for 51, 83, and 114 mm diameter 20 turn coils.

as a turn-to-turn spacer. The samples are not bonded to the holder, thereby enabling a hoop stress test after $I_c(B \parallel ab)$ is measured.

2.6. 20-turn coils in up to 17 T background field

Three 4 layer, 5 turn per layer coils were designed, fabricated, and tested to analyze the performance of the high-strength Bi-2223 tape-conductor in a configuration that closely represents an actual high-field insert-coil. In our tensile tests (section 3.1) we find a longitudinal strain limit of 0.57%. We therefore designed three coils at 51, 83, and 114 mm diameter that were designed to be limited by winding strain, critical-current, and hoop strain, respectively, as shown in figure 9. The coil-design and -fabrication is shown in figures 8(a)–(c). The conductor location was imposed using Nomex® paper, similar to the bent coil-sections in section 2.3.2. The coils were wound from bare tape and turn-to-turn insulation was provided by co-winding Nylon wire, whereas layer-to-layer insulation was provided by a polyimide sheet.

Each coil was equipped with a splice with a length of $\frac{1}{6}$ of the circumference and located at the end of the coil at the layer-to-layer transition between layer 2 and 3. A worst-case estimate (splice-cooling occurring only longitudinally along the conductor) of the heating resulting from a high splice-resistance (section 3.3), suggested a 1, 0.7, and 0.5 K temperature rise at the splice for the 51, 83, and 114 mm coil, respectively. Each splice was therefore equipped with a copper cooling-fin to provide a cooling-path from the splice directly to the helium bath as shown in figure 10 to ensure that the coils are not limited by splice-heating. Adding the cooling-fins reduced the worst-case estimated temperature-rise at the splice to 0.3 K or lower.

The coils were not impregnated and the turns are therefore self-supporting. The coils were tested at 10, 12.5, 15, and 17 T background field at 4.2 K in the 195 mm bore of the

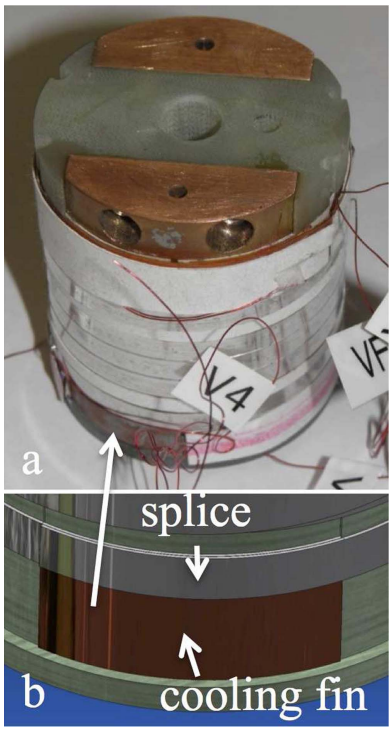

Figure 10. Photo of a finished 51 mm diameter coil (a) equipped with a copper cooling fin as drawn in (b) to conduct heat from the splice to the helium bath.

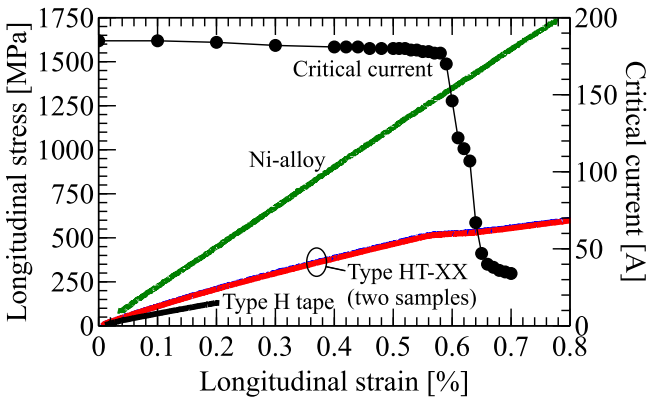

Figure 11. Applied displacement and resulting stress and $I_c(\sigma)$ in longitudinal tensile tests at 77 K.

NHMFL's Large Bore Resistive Magnet (LBRM), which was equipped with a 168 mm bore cryostat.

3. Results

3.1. Longitudinal tensile tests and thermal contraction

The $\sigma(\epsilon)$ data for two laminated DI-BSCCO HT-XX samples, the Ni-alloy lamination, and the bare tape are shown in figure 11. Included in the graph are the results of the $I_c(\sigma)$ measurement on the laminated conductor. The $\sigma(\epsilon)$ data for the DI-BSCCO HT-XX tape, until the point at which clearly yield occurs at $\epsilon = 0.57\%$ and $\sigma = 516$ MPa, can be

Table 1. Summary of the results of the longitudinal tensile tests at 77 K.

Material[a]	$\sigma_{critical}$ (MPa)	$\epsilon_{critical}$ (%)	E_{secant} (GPa)
Bi-2223 HT-NX	516	0.57	91
Ni-alloy lamination	1750	0.77	225
Bi-2223 Type H	136	0.20	62

[a] No dog-boning.

parameterized by:

$$\sigma(\epsilon) = 635.1\epsilon^3 - 930.2\epsilon^2 + 1176\epsilon - 8.431. \quad (1)$$

A summary of the critical stress ($\sigma_{critical}$) and strain ($\epsilon_{critical}$) values, as well as the secant Young's moduli (E_{secant}) is given in table 1.

The average thermal contraction of DI-BSCCO HT-XX from 295 K down to 4.2 K from 3 different measurements of the sample is $-0.27 \pm 0.03\%$, which is a close match to the -0.24% of G10 glass-fiber epoxy in the direction parallel to the glass fibers [64].

3.2. Room-temperature bending

3.2.1. Simple bending. A quick impression of the mechanical properties of DI-BSCCO HT-XX is obtained from a simple room-temperature bend until breakage, as is shown in figure 4. It is found that the conductor feels stiff and that it can withstand bending diameters below 25 mm, until breakage occurs. It is also found that the tape-sections on both sides of the failure point return to be straight, suggesting fully elastic deformation until breakage, which is similar to the brittle Ni-alloy lamination (figure 11).

3.2.2. Single- and double-bending. The results of the single- and double-bend tests (figure 5) are summarized in figure 12. The I_c at the 8 mm position is in fact the I_c measured between a voltage-tap pair between the 0 and 16 mm positions, etcetera. The samples were bent around the middle, 64 mm location. The I_c of the non-degraded samples is 190–195 A and a sample is considered degraded if a unambiguous visual reduction of the I_c in the central, bent, section occurs, corresponding to a reduction in the critical current on the order of 5 A. It is found that the I_c values for the central, bent, region start to become lower at 22.1 mm diameter in the single-bend test and at 38 mm diameter in the double-bend tests. The latter value agrees with a minimum bend-diameter of 40 mm that is specified by SEI and which stems from their double-bend tests [55].

3.2.3. Bent coil-sections. The critical-current of bent coil-sections (figure 6(a)) as a function of bend-diameter is plotted in figure 13. It is found that at least down to the 31.6 mm diameter coil-section there is only a small gradual reduction that is due to the small intrinsic and reversible strain-dependence that is typical for Bi-based superconductors

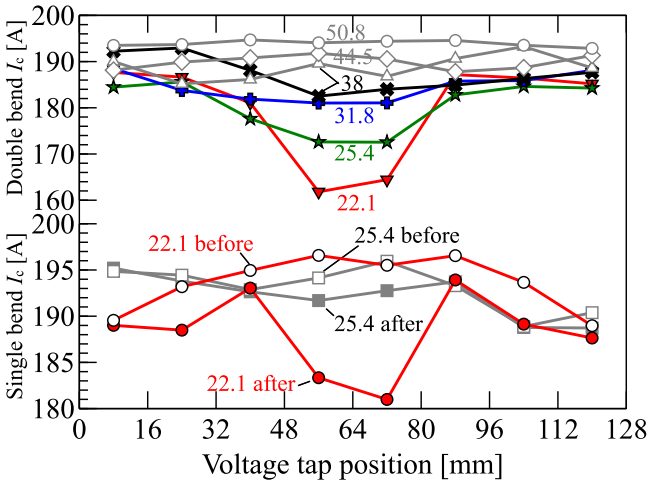

Figure 12. Critical-current at 77 K in self-field as a function of position for double-bend (top) and single-bend (bottom) tape-sections.

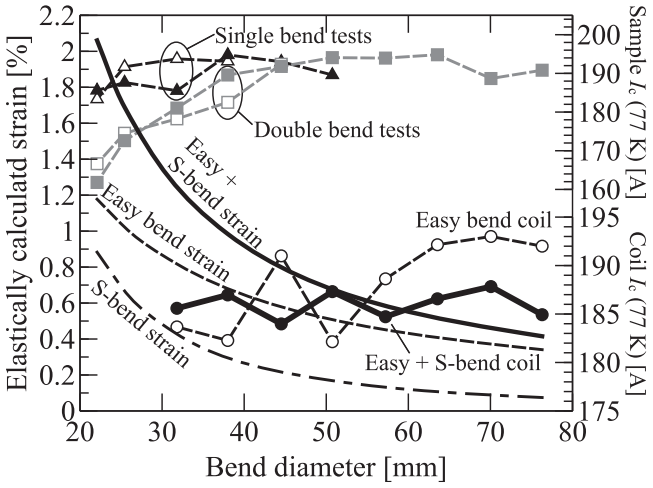

Figure 13. Summary graph of the critical-current as a function of bend-diameter for single- and double-bend tape-samples, and easy- and hard-way bend coil-sections. Included are elastically-calculated strain-levels as a function of bend-diameter.

[6, 27, 31, 36]. Included in figure 13 are the I_c values from the single- and double-bent samples at the 56 mm position. Again it is seen that the single- and double-bend I_c starts to reduce only below 25 and 40 mm, respectively.

Included in figure 13 are the elastically-calculated strain-levels as sketched for easy-way bending in figure 14 and calculated using:

$$\epsilon_{total} = \epsilon_{wind} + \epsilon_{hoop} = \frac{t}{2r} + \frac{BIr}{AE}, \quad (2)$$

in which ϵ_{total} represents the total strain, ϵ_{wind} is the strain due to bending during winding, ϵ_{hoop} is the hoop strain that results from a Lorentz load on the conductor, r represents the radius of the bend, t is the thickness or width at which the strain is calculated (for figure 13 the thickness or width of the tape), B is the magnetic field at the conductor location, I is the transport current, A is the conductor cross-section area, and E is the conductor's Young's modulus. The hoop strain is

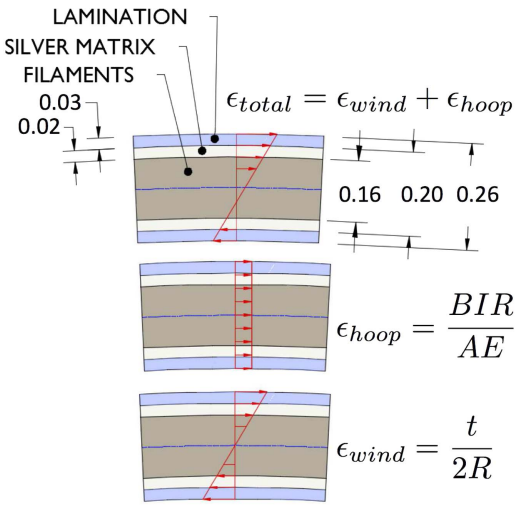

Figure 14. Schematic representation of the strain during easy-way bending including hoop strain. The relative fractions of lamination, matrix, and filaments are to scale.

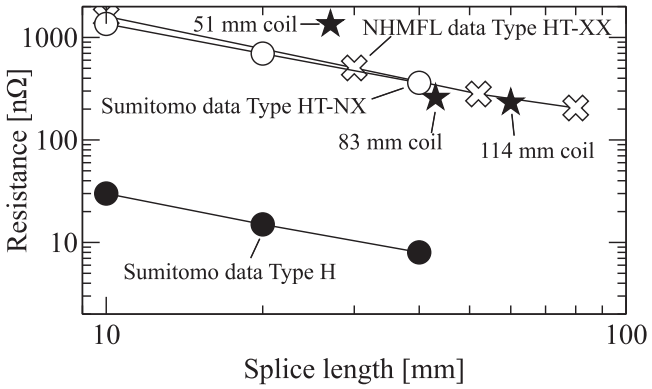

Figure 15. Summary of measured splice resistances measured at 77 K on curved splices as a function of splice length. Included are splice resistances as measured in our coils and data from SEI [60] (reproduced with permission from Sumitomo Electric Industries Ltd).

ignored for the bent coil-sections that were measured at 77 K (i.e. for the calculated strain-levels in figure 13) since the generated magnetic field is negligible.

In comparing the I_c values in figure 13 with the elastically-calculated strain-levels, it is clear that both for the single-bent samples, as well as for the bent coil-sections, the strain on the outside of the conductor approaches, or even is above 1% before the I_c starts to reduce. These values substantially surpass the 0.57% limit that was found in the longitudinal tensile-test at 77 K in section 3.1, as will be further discussed in section 4.1. A similar amplification of the mechanical limits with bending was detected in other evaluations [57], albeit not to the extend as is observed here. In the double-bend samples the I_c starts to reduce above 0.6% strain.

3.3. Splice resistance

The measured splice resistances on curved splice-samples (figure 6(b)) of various lengths at 77 K are summarized in figure 15. Included in figure 15 are data from SEI [60] on Type H and Type HT-NX DI-BSCCO as well as the splice resistances that were measured on our coils. It is seen that our data agree well with that of the straight splice-samples from SEI, and that the HT-XX resistances are more than one order larger than for the bare Type H conductor. Although the splice resistances for HT-XX are high, the worst-case expected temperature rise in typical HT-XX splices in our coils is 1 K or lower, as discussed in section 2.6. We implemented copper cooling fins in our coils, even when it is not to be expected that a 1 K temperature rise will cause a noticeable reduction in conductor performance.

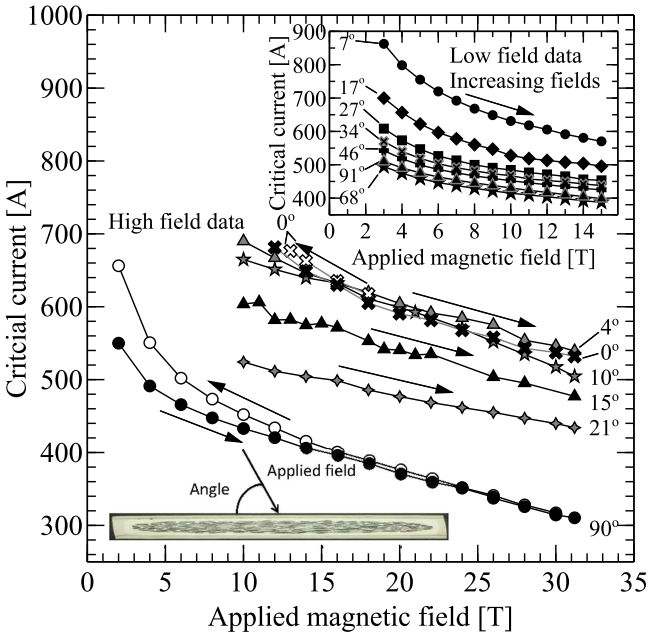

Figure 16. Critical-current of short straight samples as a function of applied magnetic field at various angles between the magnetic field and the tape. All I_c data are for increasing magnetic field, with the exception of the 0° and 90° high-field data that are plotted for increasing and decreasing magnetic field.

3.4. Critical-current measurements up to 31.2 T

3.4.1. Short straight samples at various angles. A selection of the critical-current data as measured on short straight samples is shown in figure 16. Here, we focus mainly on the increasing field results, which are the most relevant to magnet design. The well known hysteresis between the increasing and reducing field $I_c(B)$ (as indicated by the arrows) is visible in the high-field data at $\phi = 90°$. This hysteresis is commonly attributed to the presence of weak links that trap flux, thereby enhancing the effective field at the grains with increasing field and lowering the effective field at the grains with reducing field (see [65, 66] and the references therein). Scatter is seen in the high-field data for higher critical-current values. This scatter is due to the short distance between the voltage-taps of 7 mm that results in low voltage-levels in combination with the high-electromagnetic noise in a resistive magnet. A second cause for the scatter is the presence of trapped helium bubbles at high magnetic field [67] that cause temperature

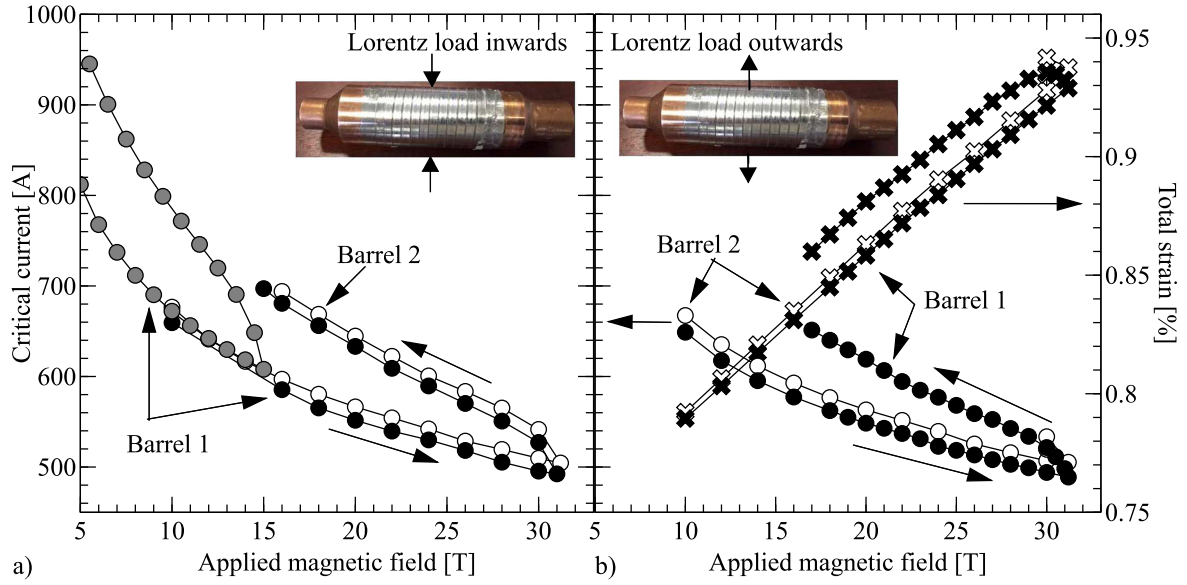

Figure 17. Critical-current as a function of magnetic field on helical samples with the Lorentz load inward (a) and outward (b).

instabilities as soon as heat is developed in the sample (e.g. during a voltage–current transition measurement).

3.4.2. Helical samples in parallel field. Two helical samples, or barrels, were prepared. $I_c(B)$ of barrel 1 was first measured in a 15 T superconducting solenoid and the I_c of barrels 1 and 2 was then measured in a resistive magnet up to 31.2 T. In both these measurements the Lorentz load was inwards, so that the tapes were supported by the G10 holders. The resulting data are summarized in figure 17(a). Significant hysteresis, amounting to about 8 T in width and much larger than for the short samples, is observed. The reason for this larger hysteresis is not entirely clear, but it could simply be volumetric, i.e. 1200 mm long samples wound as a small coil versus 35 or 45 mm long straight samples, with the long samples giving a much larger magnetization. A second origin could be that the I_c for the parallel field direction ($B \parallel ab$) is larger than for the perpendicular direction, possibly leading to a larger magnetization, although this is not evident from figure 16.

When the background magnetic field direction is switched, the Lorentz load is pointing outward and the tape is then self-supporting against the load. The $I_c(B)$ data under these conditions, as well as the elastically-calculated strains, are shown in figure 17(b). The maximum strain that is present on the outside of the tape is calculated using (2), but using (1) to translate the hoop stress, $\sigma_{hoop} = JBr$, into hoop strain ϵ_{hoop}, which is added to the winding strain $\epsilon_{wind} = 0.7\%$. This leads, at $B = 31.2$ T and the achieved sample currents to an ϵ_{total} of 0.94% for barrel 1 and to 0.95% for barrel 2. These values are significantly higher than reported by others [48, 57]. Despite these high loads, barrel 1 did not break even after 15 load-cycles, whereas barrel 2 broke at the 4th load-cycle. No degradation of the critical-current was observed before breakage of the tape, although a resistive component did appear in the voltage–current transition of barrel 2 at the 3rd load-cycle, indicative for the onset of failure.

3.5. Coil-tests in up to 17 T magnetic field

The three coils, 51, 83, and 114 mm in diameter, were successfully tested at 77 K before the high-field tests. The 51 and 114 mm coils were tested successfully in the LBRM, but the 83 mm diameter coil failed prematurely at 0.44% winding strain plus 195 MPa hoop stress, i.e. at 0.62% total strain. It was re-wound without a splice in order to save time, and successfully re-tested. Voltage–current transitions were measured in all coils at 10, 12.5, 15, and 17 T, but only the 17 T data are summarized here since these are at the highest strain-levels.

3.5.1. Results for the 51 mm diameter coil. The layer- and splice-voltages as a function of coil-current at 17 T for the first run of the 51 mm diameter coil are shown in figure 18. It is seen that the layers go into transition at almost the same time. The maximum current in the coil was 593 A which corresponds to a $\sigma_{hoop} = 219$ MPa which, using (1) and (2), translates to maximum strain-levels of $\epsilon_{total,fila} = 0.60\%$ and $\epsilon_{total,tape} = 1.02\%$ for the filaments and tape outer edge, respectively. Multiple current ramps were done but no degradation of the coil-performance was detected. In one of the consecutive runs, the coil-current was ramped to higher current resulting in a voltage-level of 10 mV that triggered the coil-protection system, and it was demonstrated that the energy (albeit for a small coil) could be safely discharged into a dump-resistor. As expected, a high splice-resistance was observed, which is consistent with figure 15.

A high-resistive component was detected in layer 1, which can be partly explained by an incorrect placement of one of the layer 1 voltage-taps so that the measured voltage includes the current terminal, as shown in the inset in figure 18. Correcting the layer 1 voltage by subtracting a

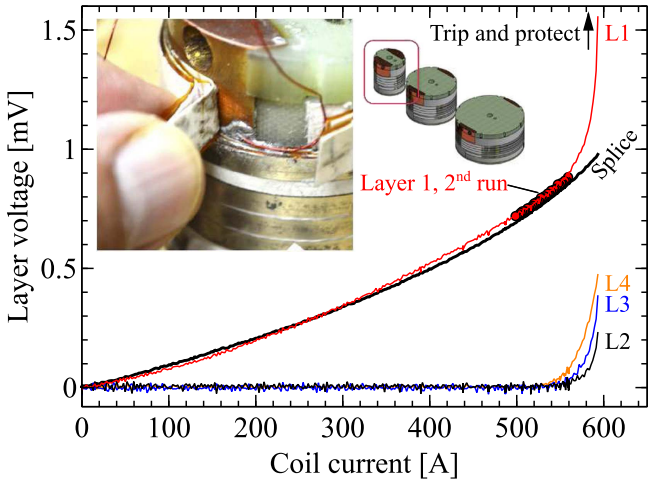

Figure 18. Layer-(L1 through L4) and splice-voltages as a function of coil-current for the 51 mm coil at 4.2 K in 17 T background magnetic field. The inset shows the incorrect location of one of the first-layer voltage-taps that includes the current-terminal.

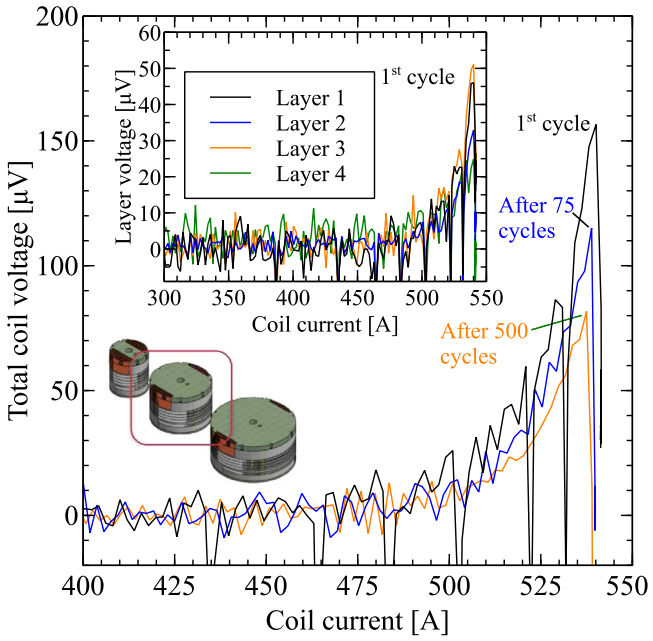

Figure 19. Inset: layer voltages as a function of coil-current for the re-wound 83 mm coil at 4.2 K and 17 T background field. Main graph: total coil-voltage as a function of coil-current during the first run and after 75 and 500 cycles.

resistive component is only partially possible, suggesting that there is a nonlinear component as well that is so far not explained. Included in figure 18 is a reproduction of part of the layer-1 voltage-trace during the second run, indicating the absence of damage after 1.02% total strain was reached on the outside of the outermost tape.

3.5.2. Results for the 83 mm diameter coil. The voltage–current traces for the layers in the (re-wound) 83 mm coil at 4.2 K and 17 T background magnetic field for the first run are shown in the inset of figure 19. The large dips in the voltage–

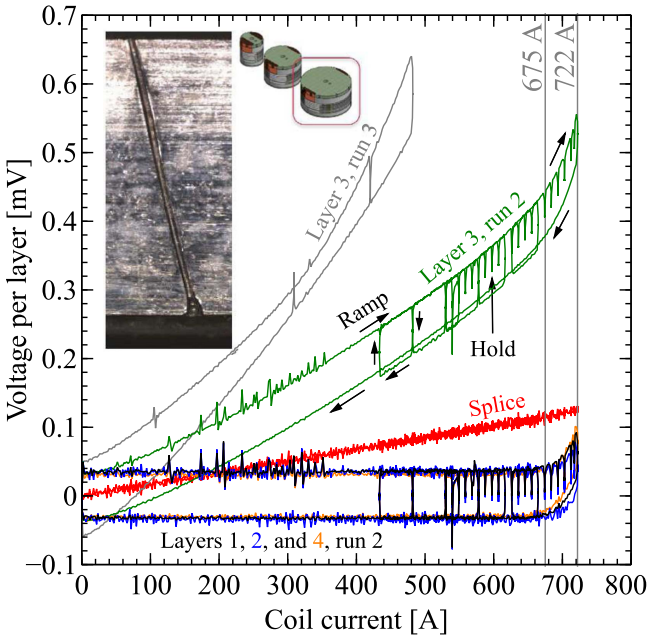

Figure 20. Layer- and splice-voltages as a function of coil-current at 4.2 K and in 17 T background field for the 114 mm coil. The inset shows a crack that was observed in the lamination in layer 3 after the coil-test.

Table 2. Strain-levels in the cyclic load-tests of the 83 mm diameter coil.

Current (A)	σ_{hoop} (MPa)	ϵ_{hoop}	ϵ_{wind}	ϵ_{total}
186	112	0.10%	0.44%	0.54%
489	293	0.29%	0.44%	0.73%

current traces are places where the current-ramp was paused. The highest current that was reached was 542 A, which translates to $\sigma_{hoop} = 325$ MPa, and, through (1) and (2) to $\epsilon_{total,fila} = 0.54\%$ and $\epsilon_{total,tape} = 0.77\%$.

Since multiple runs did not show any changes, and since the layers showed simultaneous transitions, the coil was used for cyclic load-tests to investigate the possibility for changes after a large number of cycles. During cycling, the current was ramped between 186 and 489 A, at increasing ramp-rates up to 300 A s^{-1}. As summarized in table 2, this means sweeping between 0.54% and 0.73% total strain-levels on the outside of the outermost conductor. Translated to conductor length this means between 1.4 and 1.9 mm extension along the outer conductor circumference and between 0.4 and 0.6 mm increase of the outer diameter. After 75 and 500 cycles, the voltage–current transition measurement was repeated up to 542 A and the results for the total coil-voltages are shown in the main graph of figure 19. It is seen that no reduction of the critical-current occurs even after 500 cycles. In contrast, a slight improvement is visible.

3.5.3. Results for the 114 mm diameter coil. The results of the second and third run of the 114 mm coil-test are summarized in figure 20. The inductive voltage while

Table 3. Summary of the maximum achieved strain-levels while retaining undamaged current-density and before breakage, with breakage occurring at the next higher strain level or during strain cycling. An exception is the premature failing 83 mm coil nr. 1 for which the strain at breakage is given. For experiments in bold font, no breakage was observed. For strain values in bold font, the filament strain surpasses the tensile-test limit of 0.57% strain.

						Filaments			Lamination		
Experiment	Diameter (mm)	T (K)	B (T)	I (A)	σ_{hoop} (MPa)	ϵ_{wind}	ϵ_{hoop} (%)	ϵ_{total}	ϵ_{wind}	ϵ_{hoop} (%)	ϵ_{total}
Tensile test	—	77	—	—	—	—	—	0.57	—	—	0.57
Double-bend test	38.2	77	—	186	—	0.50	—	—	0.82	—	—
Single-bend test	25.4	77	—	189	—	**0.63**	—	—	**1.02**	—	—
Helix	31.8	77	—	184	—	0.50	—	—	0.82	—	—
Helix with S-bend	31.8	77	—	186	—	**0.63**	—	—	**1.24**	—	—
Barrel sample 1	37.0	4.2	31.2	492	243	0.43	0.24	**0.67**	0.70	0.24	**0.94**
Barrel sample 2	37.0	4.2	31.2	505	249	0.43	0.25	**0.68**	0.70	0.25	**0.95**
51 mm coil	50.8	4.2	17	593	219	0.39	0.21	**0.60**	0.81	0.21	**1.02**
Failed 83 mm coil nr. 1, *breakage*	82.6	4.2	17	325	195	0.21	0.19	0.40	0.44	0.19	0.62
Rebuilt 83 mm coil nr. 2	82.6	4.2	17	542	325	0.21	0.33	0.54	0.44	0.33	0.77
83 mm coil nr. 2 cycle lower limit	82.6	4.2	17	186	112	0.21	0.10	0.31	0.44	0.10	0.54
83 mm coil nr. 2 cycle upper limit	82.6	4.2	17	489	293	0.21	0.29	0.51	0.44	0.29	0.73
114 mm coil	114.3	4.2	17	675	561	0.15	0.62	**0.77**	0.30	0.62	**0.92**

ramping current is not subtracted from the resistive voltages in order to better clarify the onset of damage. As in layer 1 of the 51 mm coil, there is a non-zero voltage present in layer 3 of the 114 mm coil. It is suspected, but not confirmed, that this is again due to a misplaced voltage-tap. Small current-ramp loops were made until the onset of the superconducting-to-normal transition occurred around 675 A and the current was then ramped in small steps until a rapid dissipative voltage increase occurred when approaching the maximum achieved current of 722 A. On the down ramp from 722 A the return voltage permanently increased, suggesting damage. As can be seen from the voltage in layer 3 in the third run, damage had indeed occurred. Inspection of the conductor after testing revealed a full width fracture in the outside lamination of the conductor in layer 3 as shown in the inset of figure 20. The inside lamination was intact.

The hoop stress at 675 A where the coil is assumed to be still undamaged, i.e. at the onset of the transition, amounts to $\sigma_{hoop} = 561$ MPa. This leads to $\epsilon_{total,fila} = 0.77\%$ and $\epsilon_{total,tape} = 0.92\%$ if the $\epsilon_{wind,fila} = 0.15\%$ and $\epsilon_{wind,tape} = 0.30\%$ winding strains are included. At the maximum-achieved current of 722 A, $\epsilon_{total,tape} = 0.97\%$, indicating that failure occurs between a total strain on the lamination of 0.92% and 0.97%. As for the helical-sample results (section 3.4.2) and the bending-tests (section 3.2) these values convincingly surpass the 0.57% strain limit that was found for in the longitudinal tensile tests (section 3.1).

4. Discussion

4.1. Achieved strain-levels

A summary of the achieved strain-levels at which no visible reduction in the critical-current is observed or conductor-failure occurs is presented in table 3. The strain-levels are calculated elastically both at the filament extremities (point 2 in figure 2) as well as at the outer edge of the conductor (point 4 in figure 2). The strain values in bold-font indicate tests where the filament strain convincingly surpasses the 0.57% longitudinal strain limit that was found in the tensile tests at 77 K (section 3.1). For the experiments in bold-font, no conductor failure was observed. In the bending and hoop stress tests, the strain on the lamination for the last datapoint where the conductor is still intact ranges from 0.92% to 1.02%, with 1.24% for the helix with an S-bend as outlier. This amplification of the strain limit in single-bending and hoop strain on DI-BSCCO HT-XX is similar to what was recently reported by others [55, 57], but the strain values are substantially larger in our observations. Larger strain limits in bending and hoop stress compared to longitudinal tension were also reported in the past for bare Bi-2223 tapes with a pure Ag matrix [68], but the explanation given then of strain-relaxation as a result of yield in the Ag-matrix does not hold for Bi-2223 that is laminated with a non-yielding outer layer, as will be discussed next.

The ultimate tensile strain for the Ni-alloy lamination from our longitudinal tensile tests is 0.77%, but it is suspected that this value is too low, since literature tensile test data for the Ni-alloy indicates that yield occurs around 1% and breakage can be postponed even to above 1.5%, depending on the heat treatment condition. This suggests that the lamination is capable of holding the brittle Bi-2223 fractions together and that filament fracture is delayed, at least until the yield strain of the lamination is reached. This reinforcement effect is notable considering the reported mechanical properties of dense Bi-2223 of $\sigma_{failure,tensile} \approx 100$ MPa, $E_{2223} \approx 70$ GPa, and specificaly $\epsilon_{failure,tensile} \approx 0.14\%$ [69, 70], and also in view of the typical 0.3%–0.4% strain limits that are commonly observed in Bi-based/Ag-alloy superconductors as discussed in our introduction.

More advanced three-dimensional mechanical modeling is presently being done in order to understand why the strain limit is so much enhanced in bending. Pending the outcome of that effort, intuitively one can imagine that bending causes a significant-transverse compression on the Bi-2223/Ag-alloy section which could be the main reason for the delayed filament fracture. One could argue that an elastically-calculated strain is not applicable here since the soft Ag/Ag-alloy fraction could yield, similar to what was previously suggested for bare Bi-2223 tapes in [68]. Examples in the literature of Nb_3Sn wires and Bi-2223 tapes that are soldered to bending-springs while simultaneously measuring the lattice-strain in the brittle superconductors using x-ray diffraction, however, suggest that strain-levels at least up to 0.8% are indeed transferred through soft intermediate layers such as solder and copper and Ag/Ag-alloy matrices [30, 71].

Since a 0.92% or larger elastic strain limit was achieved solely through bending in the single-bend tests (section 3.2), through a large winding strain of 0.7% in combination with a 0.24% hoop strain in the helical barrel samples (table 3, section 3.4.2), and through a limited winding strain of 0.30% in combination with a large hoop strain of 0.62% in the 114 mm coil (table 3, section 3.5.3), we conclude here that an elastically-calculated strain of 0.92% is the maximum permissible limit for single-bent, hoop strained DI-BSCCO Type HT-NX. A high-field coil that is wound from high-strength DI-BSCCO Type HT-NX should be limited to perhaps 0.7% strain at the conductor extremities to allow for sufficient margin, e.g. for a heating induced additional local strain during a quench.

4.2. Critical-current as a function of magnetic field and field-angle

One can argue that for a practical high-field insert-coil design the coil-current will be limited by the radial-field components. To establish the current margins in various coil-sections, and more specifically to calculate the behavior of the coil during a quench, however, the angular-(figure 16, [72]) and temperature-dependencies [45] become relevant and it is desirable to establish a parameterization of $I_c(B, T, \text{angle}[, \epsilon])$. Though the critical-current as a function of temperature at insert-coil-relevant high fields (>15 T) is not yet available, it is useful to already investigate the possibility to condense the $I_c(B, \text{angle})$ data at 4.2 K from figure 16 into a form that lends itself for parameterization.

An alternative way to summarize the results from figure 16 is to plot the critical currents as a function of angle at constant applied magnetic field. This is shown in the inset of figure 21 for the low-field data from figure 16. The closed symbols in this graph are the actual data with the sample holder (figure 7) rotated 'left' and 'right' from the $B \parallel ab$ orientation. It is instructive to investigate the amount of symmetry between the 'left' and 'right' directions. This is done by assuming that the actual peak-position is slightly left of the $B \parallel ab$ orientation and at a 1% higher I_c. The 'right' data are then mathematically flipped around the maximum and a peak-position shift is varied until the differences between 'left' and 'right' data are minimized. A shift of the peak-position of 2.6° to the 'left' is found and the (assumed) 1% higher I_c values at the peak are shown in the graph as open symbols. Although it seems apparent that the peak-position is indeed not located at the $B \parallel ab$ orientation, it is not possible to distinguish between an average texture misalignment-angle of the *c*-axis in the Bi-2223 grains in the conductor, or a potential-systematic error in the angle in the experimental setup.

The angle dependency data can be re-graphed normalized to the assumed peak-position and peak I_c-value as is done in the main graph of figure 21, in which also the high-field results are included. The main graph in figure 21 suggests that some form of parameterization of the angle dependency is possible, at least for a single temperature of 4.2 K and for fields above 10 T. The data for lower magnetic fields substantially increase the spread in the normalized plot but these data are less relevant for insert-coils that operate in a background magnetic field that is generated by LTS outer coils. Parameterization of the measured data, perhaps using one of the available models in the literature [72–75] is, however, outside of the scope of the present paper.

4.3. Tests of the 20 turn coils in 17 T background field

The initial experiment (section 2.6) aimed to operate both the 51 and the 114 mm diameter coils to failure, while the 83 mm coil would be limited by I_c, was only partly successful as a result of the unexpectedly high strain limit. Nevertheless, we were able to drive the 114 mm coil and one of the helical samples to failure. The coil tests were therefore successful, but there remain a number of concerns that are relevant for a full-scale insert-coil design.

Our main concerns are the unexpected voltages in layer 1 of the 51 mm coil and in layer 3 of the 114 mm coil, in addition to an unexplained premature failure of the first 83 mm coil. Although the unexpected voltages did not prevent the coils from surviving very high strain-values, the failure in the 114 mm coil did occur in layer 3 that also showed the unexpected voltage. It was discussed in section 3.5 that a simple linear correction, i.e. subtracting a resistive component from the unexpected layer voltages, is insufficient and a nonlinear component is also present. It is unfortunate that the exact placement of the voltage taps was not sufficiently investigated since the coils were disassembled to search for cracks before the data were fully analyzed. This, combined with the observed nonlinearity in the unexpected layer voltages plus an unclarified premature failure of the first 83 mm coil leaves uncertainties on the reliability of the coil fabrication process. Further research is needed to determine the sensitivity of the mechanical integrity of the conductor to potential-light surface damage such as scratches that might have occurred during the so-far not stringently controlled coil fabrication process.

5. Conclusions

We performed a systematic feasibility study of the suitability of high-strength DI-BSCCO Type HT-NX for high-field

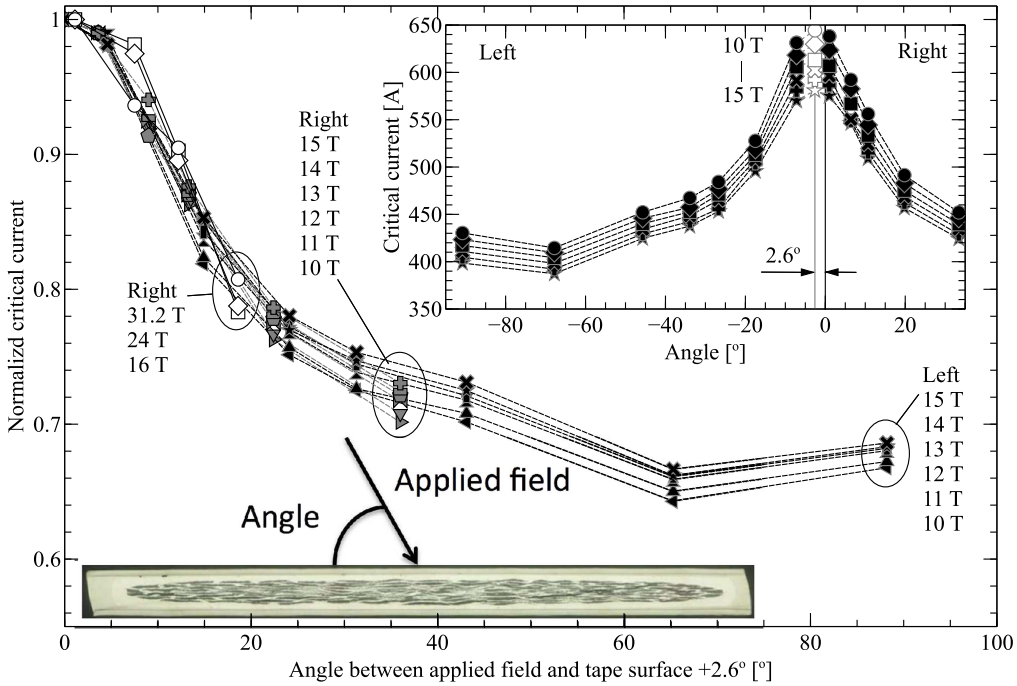

Figure 21. Critical-current as a function of field-angle for 10–15 T (inset) and normalized and shifted (as described in the main text) critical-current as a function of field-angle for 10–31.2 T.

solenoid applications by low-temperature tensile tests, single- and double-bend tests, coil sections with a single-pitch and a single-pitch plus s-bend, coil sections with a splice, helical-wound and short-straight samples tested up to 31.2 T, and 20-turn coils that were tested up to 17 T. We found a tensile stress- and strain limit of 516 MPa and 0.57%, respectively, whereas the maximum allowable stress- and strain-levels in bending, and coil-sections and 20-turn coils were substantially higher.

In three decidedly-different configurations, i.e. pure bending, small bending strain in combination with large hoop strain, as well as in large bending strain in combination with small hoop strain, we found strain limits amounting to 0.92% and larger, calculated elastically at the outer edge of the conductor.

We conclude that in coils that are exposed to a single-bend during winding in combination with hoop strain, a 0.92% strain limit seems applicable. Although this is 0.27% higher than the approximately 0.65% limit that is stated for REBCO conductors [14], the advantage of REBCO clearly is the higher stress limit if the Cu-fraction in the cross-section can be limited, which is specifically the case for no-insulation coils.

Nonetheless, the to first order comparable strength to REBCO in a multi-filamentary conductor, in combination with a sufficient current-density and magnetic-field limit, and the fact that it can be purchased reacted and insulated, render high-strength DI-BSCCO Type HT-NX highly suitable for insert-coils for high-field solenoid magnets.

Acknowledgments

This work was performed at the National High Magnetic Field Laboratory, which is supported by NSF DMR-1157490 and the State of Florida, and also benefitted from support by the National Institute of General Medical Sciences of the National Institutes of Health under Award Number R21GM111302. The authors would like to thank W W Brey, T A Cross, and L Frydman for their support and helpful discussions.

References

[1] Committee on Opportunities in High Magnetic Field Science; Solid State Sciences Committee; Board on Physics and Astronomy; Division on Engineering and Physical Sciences; National Research Council (eds) 2005 *Opportunities in High Magnetic Field Science* (Washington, DC: The National Academies Press) (https://doi.org/10.17226/11211)

[2] Committee to Assess the Current Status and Future Direction of High Magnetic Field Science in the United States; Board on Physics and Astronomy; Division on Engineering and Physical Sciences; National Research Council (eds) 2013 *High Magnetic Field Science and its Application in the United States: Current Status and Future Directions* (Washington, DC: The National Academies Press) (https://doi.org/10.17226/18355)

[3] Bruker BioSpin 2009 http://ir.bruker.com/investors/press-releases/press-release-details/2009/Bruker-Announces-Avance-1000-the-Worlds-First-1-Gigahertz-NMR-Spectrometer/default.aspx

[4] Godeke A, Cheng D, Dietderich D R, Ferracin P, Prestemon S O, Sabbi G and Scanlan R M 2007 *IEEE Trans. Appl. Supercond.* **17** 1149–52

[5] Godeke A 2005 Performance boundaries in Nb_3Sn superconductors *PhD Thesis* University of Twente doc.utwente.nl/50775/1/thesis_Godeke.pdf

[6] Bottura L and Godeke A 2012 *Rev. Accel. Sci. Technol.* **5** 25–50

[7] Godeke A, Jewell M C, Fischer C M, Squitieri A A, Lee P J and Larbalestier D C 2005 *J. Appl. Phys.* **97** 093909
[8] Dietderich D R, Kelman M, Litty J R and Scanlan R M 1998 *Adv. Cryo. Eng. Mater.* **44B** 951–9
[9] Dietderich D R and Godeke A 2008 *Cryogenics* **48** 331–40
[10] Xu X, Sumption M, Peng X and Collings E W 2014 *Appl. Phys. Lett.* **104** 082602
[11] Ayai N *et al* 2008 *Physica* C **468** 1747–52
[12] Godeke A *et al* 2010 *Supercond. Sci. Technol.* **23** 034022
[13] Larbalestier D C *et al* 2014 *Nat. Mater.* **13** 375–81
[14] Weijers H W *et al* 2014 *IEEE Trans. Appl. Supercond.* **24** 4301805
[15] Senatore C, Allesandrini M, Lucarelli A, Tediosi R, Uglietti D and Iwasa Y 2014 *Supercond. Sci. Technol.* **27** 103001
[16] Yanagisawa Y *et al* 2014 *J. Magn. Reson.* **249** 38–48
[17] Markiewicz W D *et al* 2012 *IEEE Trans. Appl. Supercond.* **22** 4300704
[18] Weijers H *et al* 2010 *IEEE Trans. Appl. Supercond.* **20** 576–82
[19] Weijers H W *et al* 2016 *IEEE Trans. Appl. Supercond.* **26** 4300807
[20] Matsumoto S, Kiyoshi T, Otsuka A, Hamada M, Maeda H, Yanagisawa Y, Nakagome H and Suematsu H 2012 *Supercond. Sci. Technol.* **25** 025017
[21] Yoon S, Kim J, Lee H, Hahn S and Moon S H 2016 *Supercond. Sci. Technol.* **29** 04LT04
[22] Awaji S, Oguru H, Watanabe K, Hanai S, Miyazaki H, Tosaka T, Ioka S, Fujita S, Diabo M and Iijima Y 2016 *Supercond. Sci. Technol.* **29** 055010
[23] Iguchi S *et al* 2016 *Supercond. Sci. Technol.* **29** 045013
[24] Piao R *et al* 2016 *J. Magn. Reson.* **263** 164–71
[25] Kametani F, Jiang J, Matras M, Abraimov D, Hellstrom E E and Larbalestier D C 2015 *Sci. Rep.* **5** 8285
[26] Jiang J, Starch W L, Hannion M, Kametani F, Trociewitz U P, Hellstrom E E and Larbalestier D C 2011 *Supercond. Sci. Technol.* **24** 082001
[27] Cheggour N, Lu X F, Holesinger T G, Stauffer T C, Jiang J and Goodrich L F 2012 *Supercond. Sci. Technol.* **25** 015001
[28] ten Haken B, Beuink A and ten Kate H H J 1997 *IEEE Trans. Appl. Supercond.* **7** 2034–7
[29] ten Haken B, ten Kate H H J and Tenbrink J 1995 *IEEE Trans. Appl. Supercond.* **5** 1298–301
[30] ten Haken B and ten Kate H H J 1996 *Physica* C **270** 21–4
[31] ten Haken B, Godeke A, Schuver H J and ten Kate H H J 1996 *IEEE Trans. Magn.* **32** 2720–3
[32] ten Haken B, Godeke A, Schuver H J and ten Kate H H J 1996 *Adv. Cryo. Eng. Mater.* **42B** 651–8
[33] Osamura K, Sugano M and Matsumoto K 2003 *Supercond. Sci. Technol.* **16** 971–5
[34] Osamura K, Machiya S, Ochiai S, Osabe G, Yamazaki K and Fujikami J 2013 *Supercond. Sci. Technol.* **26** 045012
[35] Osamura K, Machiya S, Hampshire D P, Tsuchiya Y, Shobu T, Kajiwara K, Osabe G, Yamazaki K, Yamada Y and Fujikami J 2014 *Supercond. Sci. Technol.* **27** 085005
[36] Godeke A, Hartman M H C, Mentink M G T, Jiang J, Matras M, Hellstrom E E and Larbalestier D C 2015 *Supercond. Sci. Technol.* **28** 032001
[37] Cheggour N, Stauffer T C, Jiang J and Jewell M C 2016 Are densified Bi-2212 wires more strain resilient? *Presented at the 2016 Low Temperature Superconductor Workshop (Sante Fe, NM, 9 February)*
[38] Damborsky K and Parrell J 2015 *Supercond. Sci. Technol.* **28** 050501
[39] Bjoerstad R, Scheuerlein C, Rikel M O, Ballarino A, Bottura L, Jiang J, Matras M, Sugano M, Hudspeth J and Di Michiel M 2015 *Supercond. Sci. Technol.* **28** 062002
[40] Otto A and Saraco L 2016 Strong 2212 wires *Presented at the 2016 Low Temperature Superconductor Workshop (Sante Fe, NM, 9 February)*
[41] Matras M, Jiang J, Trociewitz U P, Hellstrom E E and Larbalestier D C 2015 A practical process to densify high-temperature superconducting $Bi_2Sr_2CaCu_2O_{8+x}$(2212) round wire before coil winding *US Patent disclosed*
[42] Trociewitz U P, Chen P, Hilton D K, Bosque E S, Abraimov D V, Starch W L, Jiang J, Matras M, Hellstrom E E and Larbalestier D C 2016 A practical superconducting electrical joint design for high-temperature superconducting $Bi_2Sr_2CaCu_2O^{8+x}$(Bi-2212) round wire *US Patent pending, 62129266, March 2015*
[43] Kandel H, Lu J, Jiang J, Chen P, Matras M, Craig N, Trociewitz U P, Hellstrom E E and Larbalestier D C 2015 *Supercond. Sci. Technol.* **28** 035010
[44] Chen P, Trociewitz U P, Dalban-Canassy M, Jiang J, Hellstrom E E and Larbalestier D C 2013 *Supercond. Sci. Technol.* **26** 075009
[45] Kitaguchi H, Takahashi K, Kumakura H, Hayashi T, Fujino K, Ayai N and Sato K 2009 *Supercond. Sci. Technol.* **22** 045005
[46] Otto A, Harley E J and Mason R 2005 *Supercond. Sci. Technol.* **18** S308–12
[47] Otto A, Podtburg E, Mason R and Antaya P 2007 *IEEE Trans. Appl. Supercond.* **17** 3071–4
[48] Miyoshi Y, Nishijima G, Kitaguchi H and Chaud X 2015 *Supercond. Sci. Technol.* **28** 075013
[49] Awaji S, Oguro H and Watanabe K 2016 *IEEE Trans. Appl. Supercond.* **26** 4701104
[50] Bascuñán J, Kim W, Hahn S, Bobrov E S, Lee H and Iwasa Y 2007 *IEEE Trans. Appl. Supercond.* **17** 1446–9
[51] Hahn S, Bascuñán J, Lee H, Bobrov E S, Kim W, Ahn M C and Iwasa Y 2009 *J. Appl. Phys.* **105** 024501
[52] Yanagisawa Y *et al* 2010 *J. Magn. Reson.* **203** 274–82
[53] Hashi K *et al* 2015 *J. Magn. Reson.* **256** 30–33
[54] Kinoshita K 2014 HTS wire development and industrialization at Sumitomo *Presented at the 1st Workshop on Accelerator Magnets in HTS (Desy, Hamburg, 21 May)*
[55] Nakashima T, Yamazaki K, Kobayashi S, Kagiyama T, Kikuchi M, Takeda S, Osabe G, Fujikami J and Osamura K 2015 *IEEE Trans. Appl. Supercond.* **25** 6400705
[56] Miyoshi Y, Nishijima G, Kitaguchi H and Chaud X 2015 *Physica* C **516** 31–5
[57] Yanagisawa Y *et al* 2015 *Supercond. Sci. Technol.* **28** 125005
[58] Kuroda T *et al* 2005 *Physica* C **425** 111–20
[59] Yamada Y, Nishijima G, Osamura K, Shin H S, Goldacker W, Breschi M and Ribani P 2016 *Supercond. Sci. Technol.* **29** 025010
[60] Osabe G *et al* 2016 Development of high strength Ag-sheath Bi-2223 wire *Presented at the 2016 Workshop on Mechanical and Electromagnetic Properties of Composite Superconductors (MEM2016) (Tallahassee, FL, 22 March)*
[61] Godeke A, Chlachidze G, Dietderich D R, Ghosh A K, Marchevsky M, Mentink M G T and Sabbi G L 2013 *Supercond. Sci. Technol.* **26** 095015
[62] Bruzzone P 1995 *The 2nd Round of Strand Bench Mark Tests, July 94–August 95, JCT Final Report* ITER JCT
[63] Godeke A, Bish P, Diederich D R, Gorham C S, Hafalia A R, Higley H C, Liggins N L, Mentink M G T and Sabbi G L 2012 *AIP Conf. Proc.* **1435** 209–16
[64] Ekin J W 2006 *Experimental Techniques for Low-Temperature Measurements* (New York: Oxford University Press)
[65] Goodrich L F and Stauffer T C 2001 *J. Res. Natl. Inst. Stand. Technol.* **106** 657–90

[66] Shibutani K, Wiesmann H J, Sabatini R L, Suenaga M, Hayashi S, Ogawa R, Kawate Y, Motowidlo L and Haldar P 1994 *Appl. Phys. Lett.* **64** 924–6
[67] Bai H, Hannahs S T, Markiewicz W D and Weijers H W 2014 *Appl. Phys. Lett.* **104** 133511
[68] Weijers H W, Yoo J M, ten Haken B and Schwartz J 2001 *Physica* C **357–360** 1160–4
[69] Passerini R, Dhallé M, Giannini E, Witz G, Seeber B and Flükiger R 2002 *Physica* C **371** 173–84
[70] Oduleye O O, Penn S J and McN Alford N 1998 *Supercond. Sci. Technol.* **11** 858–65
[71] ten Haken B, Godeke A and ten Kate H H J 1997 *Adv. Cryo. Eng. Mater.* **42B** 1463–70
[72] Sunwong P, Higgins J S and Hampshire D P 2010 *J. Phys.: Conf. Ser.* **234** 022013
[73] van der Meer O, ten Haken B and ten Kate H H J 2001 *Physica* C **357–360** 1174–7
[74] Zhang M G, Lin L Z, Xiao L Y and Yu Y J 2003 *Physica* C **390** 321–4
[75] Weijers H W 2009 High-temperature superconductors in high-field magnets *PhD Thesis* University of Twente doc.utwente.nl/61648/1/thesis_H_Weijers.pdf